SCALE EFFECTS IN HYDRAULIC MODEL TESTS OF ROCK PROTECTED STRUCTURES

by

Emmett M. O'Loughlin, S. C. Mehrotra,
Y. C. Chang, and John F. Kennedy

Sponsored by
Iowa Highway Research Board
Grant No. HRB-119

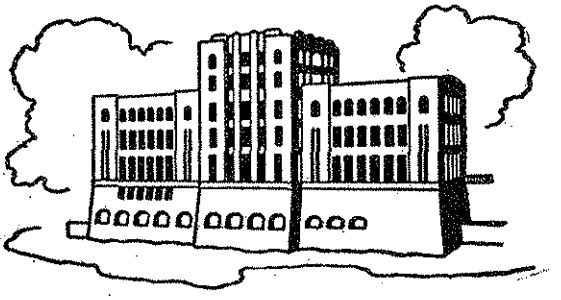

IIHR Report No. 124

Iowa Institute of Hydraulic Research
The University of Iowa
Iowa City, Iowa

February 1970

SCALE EFFECTS IN HYDRAULIC MODEL TESTS OF ROCK PROTECTED STRUCTURES

by

Emmett M. O'Loughlin, S. C. Mehrotra,
Y. C. Chang, and John F. Kennedy

Sponsored by
Iowa Highway Research Board
Grant No. HRB-119

IIHR Report No. 124

Iowa Institute of Hydraulic Research
The University of Iowa
Iowa City, Iowa

February 1970

TABLE OF CONTENTS

LIST OF FIGURES

ABSTRACT

A laboratory investigation was undertaken to determine the limiting model Reynolds number above which the scour behavior of rock protected structures can be reproduced in hydraulic models scaled according to the Froude criterion. A submerged jet was passed over an initially full scour pocket containing uniform glass spheres and the rate of scour was measured as a function of time. The dimensions of the scour pocket and jet and the particle diameters were varied as needed to maintain strict geometric similarity. For each of two different Froude numbers the Reynolds number was varied over a wide range. The normalized scour rate was found to be practically independent of the Reynolds number, $\bar{R}$, (based on the jet velocity and particle diameter) at values of $\bar{R}$ above about 2.5×10^3, and to decrease with $\bar{R}$ at smaller values. A grid placed in the jet was found to have a very strong effect on the scour rate. In an attempt to explain the effect of $\bar{R}$ on the scour behavior, turbulent pressure and velocity fluctuations were measured in air flows and water flows, respectively, over rigid scour pockets having the same geometry as those formed in the scour experiments. The normalized spectra of the fluctuations were found to be nearly independent of $\bar{R}$, but the flow pattern was found to be very sensitive to the inlet condition, the jet deflecting upward or downward in a not wholly explainable manner. This indicates that scour behavior can be modelled only if the approach flow is also accurately modelled.

Scale Effects in Hydraulic Model Tests of Rock Protected Structures

I. INTRODUCTION

It is seldom if ever possible in reduced scale hydraulic model tests to achieve complete dynamic similarity of all forces present in the prototype. The investigator must generally judge which classes of forces are dominant and design the model to preserve similarity of those forces. The unscaled forces do, to be sure, affect the model results to some extent, but the magnitude and importance of these effects is generally unknown. Reported herein are the results of an investigation conducted for the purpose of determining and quantifying scale effects associated with viscosity in an erodible bed model of rock-protected structures scaled according to the Froude law. The study was confined to the common modelling situation in which the investigator is concerned with the behavior of riprap subjected to highly turbulent flows. Such conditions are encountered frequently at or near free overfalls, outlet works, channel structures, etc. While the dynamic behavior of the fluid flow can be modelled on the basis of the familiar Froude criterion, provided the dominant forces are those associated with gravity and inertia, it is well known that the forces tending to move individual rocks may be influenced at model scale by viscous effects which are dynamically dissimilar to those occurring in the prototype. It has been the purpose of this study to detect the limitations of model scale reduction beyond which the Froude modelling criterion cannot be accepted without serious reservation.

The bulk of the experimental observations in connection with separate aspects of the study has been presented by Mehrotra [1] and Chang [2]. These authors also have given detailed descriptions of the experimental apparatus and procedures used; some duplication of this information is contained in the present report where continuity so indicates. The published observations of Mehrotra and Chang are supplemented herein by previously unreported work carried out by these investigators and by other research assistants at the Iowa Institute of Hydraulic Research.

Two types of experiments were conducted. In the first series of experiments, a water jet was passed over an erodible bed and the scour rate was measured. The flow velocity, particle size, and boundary dimensions were altered between successive experiments in order to maintain geometrical similarity and obtain a systematic variation of the Froude and Reynolds numbers. In the second series, rigid-boundary experiments were conducted in an attempt to explain certain observations made in the course of the scour experiments.

II. CHOICE OF EXPERIMENTAL CONFIGURATION

A laboratory investigation of scale effects in models of rock-protected structures must be carried out in a setup which is sufficiently general that the essential features of prototype flows over riprap are represented. These features include: (1) A high velocity flow, generally jet-like in nature and with Froude number in excess of unity; (2) Passage of the flow from a fixed boundary region onto a rock-protected zone; (3) Flow passage from the rock-protected zone at a lower velocity, often with Froude number less than unity.

Other features required in a generalized model relate to the properties of the model material used to represent rock protection. These may be specified as follows: (1) The model size should bear a relationship to the material size such that it is representative of a rock-protected structure; and (2) The particle shape must be reproducible at different model scales.

The geometry of the model, presented schematically in figure 1, and the bed material were chosen to satisfy these stipulations. An additional constraint imposed on the model geometry was the elimination of a free surface over the rock bed; the complications of the interaction between the scour profile and the free surface were thereby avoided.

III. SCOUR EXPERIMENTS

A. Selection of Variables. Experiments were conducted in an attempt to observe the nature and magnitude of viscous scale effects on a

significant and readily measurable characteristics of scour: the weight of material scoured from an erodible bed section in a specified period by a submerged horizontal jet of water. The geometric configuration is shown in figure 1. The variables pertinent to the problem may be presented in non-dimensional form as

$$\frac{W}{BL^2\gamma_s} = f\left(\frac{d}{h}, \frac{h}{L}, \frac{h}{h_1}, \frac{B}{L}, \frac{\gamma}{\gamma_s}, \frac{Vd\rho}{\mu}, \frac{V}{\sqrt{\left(\frac{\gamma_s-\gamma}{\rho}\right)d}}, \frac{Vt}{h_1}\right) \qquad (1)$$

in which the symbols have the following meaning:

W = weight of material scoured up to time t
d = particle diameter
γ_s = specific weight of particles
γ = specific weight of fluid
μ = dynamic viscosity of fluid
ρ = mass density of fluid
V = jet efflux velocity

The quantities h, h_1, L and B are defined in figure 1, and t represents time.

The set of dimensionless geometric ratios, $\frac{d}{h}$, $\frac{h}{L}$, $\frac{h}{h_1}$, and $\frac{B}{L}$, is denoted by $\bar{G}$ and, except as otherwise indicated subsequently, has been kept constant in all experiments.

Equation 1 is re-written symbolically as

$$\bar{W} = f(\bar{G}, \bar{Y}, \bar{R}, \bar{F}, \bar{T}) \qquad (2)$$

where

$$\bar{W} = \frac{W}{BL^2\gamma_s} = \text{dimensionless weight of scoured material}$$

$$\bar{Y} = \frac{\gamma_s}{\gamma} = \text{ratio of specific weights}$$

$$\bar{R} = \frac{Vd\rho}{\mu} = \text{Reynolds number}$$

$$\bar{F} = \frac{V}{\sqrt{\left(\frac{\gamma_s - \gamma}{\rho}\right)_d}} = \text{Froude number}$$

$$\bar{T} = \frac{Vt}{h_1} = \text{non-dimensional time parameter.}$$

The scour study was aimed at observing the effect of $\bar{R}$ on $\bar{W}$. The scope of the experiments was extended by making repeated observations of $\bar{W}$ over a wide range of $\bar{T}$ for two values of $\bar{F}$. The remaining quantities, $\bar{G}$ and $\bar{Y}$, were kept constant insofar as practicable.

B. Experimental Apparatus. The model geometry adopted is depicted in figure 1. Most of the water flow experiments were conducted in the glass-walled flume housed in the Institute Annex. The flume is 18 inches wide, 42 inches deep, and 15 feet long. A detailed description of the flume is presented by Rouse [3] and therefore is omitted here. Some of the larger scale experiments which could not be carried out in the 18-inch wide flume because of its limited width were conducted in a wooden flume constructed expecially for these experiments. The wooden flume was 36 inches wide, 18 inches deep, and 10 feet long. Though the relative dimensions of the scour pockets in the wooden and glass flumes were the same, there were two principal differences in the condition obtained at the approach section. First, whereas the inlet to the head tank of the glass-walled flume comprised two pipes discharging horizontally into the base of the head tank, the inlet to the head tank of the wooden flume was a single pipe discharging vertically upward from below. Second, the head tank of the glass-walled flume was very much larger than that of the wooden flume; consequently there was a much longer transition for the flow before it entered the test section in the glass-walled flume than in the wooden flume. The two differences combined to produce a higher turbulence level in the entering flow of the wooden flume. This was quite apparent after a comparison of the free surfaces in the two head tanks was made.

The only accessories used in the investigation were a pitot tube for velocity measurement in the jet throat, a manometer for determining the head difference across the orifice meter used for discharge measurement, a stop watch for time measurement, a thermometer for temperature readings, a basket for the collection of the scoured beads from the pocket, and a

scale for determining the weight of the scoured material.

Uniform, spherical glass particles were chosen for the study; the spherical shape insured complete similarity of particle shape between different experiments. Six different particle diameters were used: 3, 4, 6, 10.1, 12.7, and 15 mm. The absolute dimensions of the scour pocket, jet height, and conduit height downstream from the scour pocket were adjusted as needed for each sediment size to yield the required geometric similarity.

C. A Brief Description of the Experimental Procedure. An arbitrary value of $\overline{F}$, based on a jet velocity which produced a reasonable rate of scour, was first chosen. This value of $\overline{F}$ was held constant for all model scales in a series of experiments. For a given scale, the jet velocity and discharge were computed. During the course of each experiment, the scoured beads were collected in a basket at times chosen such that the interval between them became progressively longer as the scouring continued. The collected beads were weighed after they had dried.

Time was measured from the instant when the first few beads were scoured. The scouring commenced at a flow which was less than the desired flow. Some time would, of necessity, elapse before the final flow could be established. This time is referred to as the period of flow establishment. The velocity of the jet was measured with a pitot tube and checked against the value computed from the measured discharge. For each model scale at least two runs were made to ascertain if the results agreed within the limits of experimental errors. The water temperature was noted in each run for use in obtaining the dynamic viscosity.

The average length of each run was about 3 hours. It should be pointed out that the scouring had not altogether stopped when a run was terminated.

IV. RESULTS OF SCOUR EXPERIMENTS

A. Analysis and Plotting of Data. The cumulative weight W of the material scoured up to time t and the time t are quantities that have been directly measured. In order to plot them in the most significant manner, certain derived quantities are computed. Let $W' = \frac{W}{B}$ be the weight of the material scoured per unit width of the pocket up to time t. A characteristic

depth of scour is then given by $\sqrt{W'/\gamma_s}$. The weight is expressed as a length in order to facilitate comparison of the results of the present study with those obtained in similar studies by other investigators who chose a scour-hole dimension as the dependent variable. In dimensionless terms, the ratio of this derived length to the length of the erodible bed is simply $\sqrt{\bar{W}}$.

To study the effect of $\bar{R}$ on the $\sqrt{\bar{W}}$ - $\bar{T}$ relationship, $\sqrt{\bar{W}}$ has been plotted on arithmetic scale and $\bar{T}$ plotted on logarithmic scale on a single diagram for all the model scales in each series of experiments with constant $\bar{F}$. Plots corresponding to the two series of experiments carried out by Mehrotra [1] using two different values of the Froude number are shown in figures 2. For many model scales, Mehrotra carried out two runs at each value of $\bar{R}$ and $\bar{F}$ to check reproducibility of results. The results of all runs have been plotted in figures 2.

Several runs were made to observe the long-term scour behavior; $\sqrt{\bar{W}}$ vs. $\bar{T}$ curves for these runs have been plotted in figure 3. The curves are presented in diagrams separate from figures 2 because small but significant changes were made in the experimental setup between runs; these changes, although affecting only the headtank geometry, were sufficient to invalidate comparison of these runs with those shown in figures 2. Further discussion of this point is given in a later section.

B. Experimental Results. For the geometry chosen, and within the range of time of experiments, a characteristic depth of scour as expressed by $\sqrt{\bar{W}}$ is seen in figures 2 and 3 to vary only approximately as the logarithm of time. Laursen [4] has observed that certain geometric features of scour holes vary as log t at large values of t.

The scouring phenomenon, for the particular flow conditions and experimental geometry investigated, was essentially two-dimensional. Therefore, adhering to only two-dimensional geometrical similarity, as was done in the case of the two largest models (see note in figure 1), did not lead to any appreciable error. Both Mehrotra [1] and Chang [2] have discussed this point at length.

The significance of the Froude number in phenomena of the type under investigation is verified. Indeed, above a certain value of the

Reynolds number ($\bar{R} > 2.5 \times 10^3$, approximately) the scouring is governed almost exclusively by the Froude number. This is evidenced by the fact that points corresponding to larger model scales (6 mm, 10.1 mm, 12.7 mm, and 15 mm beads) fall nearly on a single curve in the $\sqrt{\bar{W}} - \bar{T}$ plane in figures 2. However, the curves are different for each values of $\bar{F}$. Deviations of the points become significant for values of $\bar{R}$ below approximately 2.5×10^3. The points on the $\sqrt{\bar{W}} - \bar{T}$ plane corresponding to 3 mm beads for both series of experiments ($\bar{F} = 2.53$ and $\bar{F} = 3.14$) and those corresponding to 3 mm and 4 mm beads for the $\bar{F} = 2.53$ series of experiments fall on curves which are markedly below the unique curve described by larger scales and Reynolds number. These anomalies stem from the scale effects, and are seen to act in a direction to diminish the rate of scour. With increasing $\bar{R}$, and consequently with diminishing scale effects, the depth of scour at any $\bar{T}$ increases.

C. Discussion of Results. A linear relationship between $\sqrt{\bar{W}}$ and log $\bar{T}$ would be expected only if the successive scour profiles at various times showed geometric affinity to each other, as discussed by Laursen [4]. This was certainly not the case during the early stages of scouring in the present experiments. Thus the curvature shown in some regions of figures 2 and 3 need not be further pursued.

The apparent scale effects exhibited in the smaller models is more puzzling. One is tempted to predict that there would be a tendency for the spheres to scour more readily in the smaller models than in the larger ones, because the flow should impose on the smaller spheres relatively larger drag and lift forces. The basis for this conjecture lies in the known trend of increasing drag coefficient, C_D, with decreasing Reynolds number for bodies of this shape. Reynolds numbers calculated on the basis of jet efflux velocity and particle diameter are below 2.5×10^3 in those runs where apparent scale effects are manifested; this value may be as much as an order of magnitude greater than the Reynolds number based on local velocity at the particle level. Thus we would expect significant differences in drag coefficient values between the extreme scales tested. Attendent differences in scour quantities, however, were not observed. The trends which were observed were obviously brought about by other factors large enough to outweigh the effect of increases in C_D.

It was suspected that variations in eddy size and frequencies from one model scale to another may play an important part in determining scour behavior. Accordingly, a pair of runs was made in which flow from the head-tank passed through a coarse grid screen before issuing over the erodible material. Details of the screen are shown in figure 4 together with the $\sqrt{\bar{W}} - \bar{T}$ points computed from the observations; for comparison, the points for the runs made without the screen are shown in the same diagram. The differences shown between runs with and without the screen are far greater than any previously observed in figures 2. Scour with the screen in position was almost an order of magnitude smaller than without the screen. The screen no doubt imposed a fairly uniform field of small eddies on the mean flow, but it may also have had the effect of breaking up eddies of much larger scale than the screen grid spacing. The supplimentary runs plotted in figure 4 therefore gave neither support nor contrary evidence to the aforementioned hypothesis concerning the effect of eddy structure on scour phenomena. These runs did, however, demonstrate the extreme sensitivity of the scour rate and absolute scour depth to the internal characteristics of the submerged jet.

The observations made during these supplementary tests led to the program of additional testing described in Section IV of this report.

In the extended duration tests, the flow was continued for about ten times as long as in the case of the experiments summarized in figures 2. Scour was still progressing when the runs were terminated, but at an extremely slow rate. The interval between the final two experimental points for $d = 15$ mm in figure 3 represents 29 percent of the test duration but only one percent of the scour depth. The average rate of scour during the final 10 hours of the run was five particles per hour. In the run for the smaller scale (6 mm particles) shown in figure 3, there is some indication that a scour depth asymptote is being approached. For both of the experiments summarized in figure 3 the scour rate is seen to be proportional to $\log \bar{T}$ at large times.

For the purpose of the present study, there was little point in extending these tests for longer durations.

V. INVESTIGATION OF THE ROLE OF TURBULENCE

A. Purpose of Experiments. The foregoing description of the results of the scour experiments permit the following statements to be made:

1. Small but systematic differences in a characteristic scour depth are observable in a set of geometrically similar models operated over a wide range of Reynolds numbers.
2. The difference between models diminishes to zero when the particle Reynolds number exceeds a lower limit.
3. These scale effects are opposite in direction to what might be expected on the basis of the known relationship between drag coefficient and Reynolds number for spheres in fluids of infinite extent.
4. Perturbations in the eroding jet, such as those induced by a grid, result in drastic modifications of the scour rate.

The extreme importance of the turbulence velocities in dislodging and entraining sediment particles was pointed out in the now classical experiments conducted by White [5]. His observations together with the conclusions derived from the scour experiments led to a set of experiments conducted to determine whether the Reynolds number effect could be attributed to changes in the unsteady, turbulent features of the flow. Pressure fluctuations were measured in the smaller water flume at the surface of a smooth, rigid concrete bed. The shape of the bed was the same two-dimensional form which was observed in one of the scour experiments with 15 mm particles after a long period of time. A range of flow velocities was investigated using this bed geometry. Turbulence velocities were measured in a wind tunnel for two different geometrical configurations, corresponding to 6 mm and 15 mm particle diameters. The profiles of the smooth, concrete "scour section" duplicated that observed in the scour experiments. The range of Reynolds number investigated in each of these experiments included the range studied in the scour experiments. A definition sketch for these experiments is presented in figure 5.

B. Data Acquisition and Analysis. Those quantities describing the internal flow structure which were measured include the temporal-mean velocity distribution, distribution of R.M.S. of velocity fluctuations at selected points, spectral density function of velocity fluctuations near the base of the scour hole in the air model, and spectral density function of pressure fluctuations at the base of scour hole in the water model.

Mean velocities were determined by the use of conventional Prandtl-Pitot tubes and precision alcohol or water manometers. Turbulence velocities were measured with the IIHR Old Gold Model hot wire anemometer described by Glover [6]. The spectral density functions of the pressure and velocity fluctuations were computed from the digitized outputs of a half-inch diameter Statham 2.5 psi temperature compensated pressure transducer and the hot wire anemometer. The pressure transducer output was linear with a calibration factor of 1.422 microvolts per volt per psi. Analog outputs were amplified before being digitized and stored in core of an IBM 1800 Data Acquisition and Control System; interfacing circuitry associated with the IBM 1800 consisted of a 16-point multiplixer and an analog-to-digital converter with sample-and-hold amplifiers. The sampling interval was program controlled, and could be varied in steps of one eighth of a millisecond.

The program used in collection of the pressure fluctuations data was designed originally for analyzing velocity fluctuations; the drift characteristics of the hot wire being developed at that time for use in water required that all sampling be completed in a period of no longer than one minute. Consequently, the data acquisition program was developed to yield the autocovariance function in real time, and the spectral density function could then be computed at leisure by standard transform techniques. In practice, rapid fouling of the hot wire precluded all hope of measuring velocity fluctuations in the water model, so efforts were diverted towards the analysis of pressure fluctuations at the bottom of a smooth, concrete model of the scoured bed placed in the scour pocket in the 18-inch wide flume. The real-time autocovariance program was retained and used for these measurements, and because drift was no longer a problem, integration time was extended to 240 seconds.

It is noteworthy that the program for real-time autocovariance analysis utilized quadruple precision arithmetic (64-bit words), and could accept samples at 12 millisecond intervals if the maximum lag was 99 times the sampling interval, or at 6 millisecond intervals if the maximum lag was 49 times the sampling interval. Fast Fourier Transform techniques would have allowed some improvement on this performance, although it was not necessary for the present application.

Because the frequencies of interest in the measurement of velocity fluctuations in the air tunnel were much higher than in the water model, real-time computation of the autocovariance function was not possible. This presented no inconvenience because the air-flow version of the hot wire anemometer was quite stable. The procedure adopted was developed by Dr. Locher of the IIHR staff, who separated the procedures for taking samples and computing products. Locher's program took samples successively at a specified delay time up to the limit of the IBM 1800 core capacity; auto-covariance computations were then carried out, the results stored in core, and the procedure was repeated until sufficient samples were obtained to define a spectrum with narrow confidence interval.

Further detailed information on all aspects of the data acquisition and analysis are given by Chang [2].

C. Pressure Fluctuation Measurements in Water Model. The pressure cell was mounted flush with the scour bed model and placed on the centerline at a point three-fourths of the length of the scour pocket from the upstream end. Four different velocities were used in this investigation; one was the discharge corresponding to the flow condition that produced the bed profile, two were smaller, and one was larger. The smallest discharge was limited by the magnitude of the pressure signal generated. The normalized spectral density functions of pressure fluctuations are shown in figure 6. The quantity $p'(f)$ in the ordinate of figure 6 is defined as follows:

$$p'(f) = \int_{-\infty}^{\infty} \frac{C(\tau)}{C(0)} e^{i2\pi f\tau} d\tau = \text{normalized spectral density function}$$

where

$C(0) = \overline{X(t)\ X(t)}$ = mean square of random signal X

$C(\tau) = X(t)\ X(t + \tau)$ = mean autocovariance function

f = frequency

The Reynolds numbers, $\bar{R}$, in this and subsequent diagrams are calculated using jet opening, h_1, and jet velocity, V. Each of the spectra in figure 6 are based on 8,000 samples measured with a delay of 30 milliseconds. With a maximum lag of 2.97 seconds, the spectral estimates are, at the 95 percent confidence level, within 0.95 db of true values. It is seen that there is no systematic difference among the normalized spectra for the different discharges.

D. Measurements in Air-Tunnel Model. Velocity distributions were measured at the entrance and at four sections in the larger (24 inch) model, and at three sections in the smaller (9.6 inch) model. In both models, the jet velocity was slightly nonuniform, an effect ascribed by Chang [2] to asymmetry of the geometry.

The normalized mean-velocity and turbulence-intensity distributions for four different discharges investigated in the 24-inch model are shown in figure 7 for the four stations. It is seen that for three of the discharges, the high velocity core generally paralleled the lower boundary, apparently limiting the separation eddy to the downstream end of the scour hole. For one of the discharges, that for $\bar{R}_1 = 8.6 \times 10^4$, the high velocity core separated from the lower boundary at the lip of the jet outlet, producing a larger separation eddy in the scour hole.

The downward deflection of the jet was probably caused by the Coanda effect. The change of direction on the lower boundary causes the surface pressure to be lower than that of the surroundings. The pressure force is related to the centrifugal acceleration associated with the curved flow, and keeps the jet attached to the boundary. The range of entrance velocity for which the jet went up instead of down toward the scour hole was found, with the help of smoke generated by burning oil, to be between 38.2 fps and 64.3 fps. Outside this range, the normalized velocities and turbulence intensities for different discharges were nearly identical.

The velocity and turbulence-intensity distributions for five different discharges in the 9.6-inch model (see figure 5) are shown in

figure 8. It was found that the high velocity core of the jet always followed the lower boundary, and the nonuniqueness of the flow pattern observed in the 24-inch model was not found to occur in this model. The normalized velocity distributions for four different discharges are seen to nearly coincide, only the lowest discharge deviating slightly. The distribution of the normalized turbulence intensity for this case is also seen to differ from the other four.

Supplementary observations were made in the water model to detect whether separation at the jet lip occurred; no such flow separation was observed.

E. Spectral Density Functions of Velocity Fluctuations. To explore the turbulence structure of the flow in the scour hole, a point located about one-fourth of the jet-opening height from the bed, approximately three-fourths of the scour hole length from the upstream end of each scour-pocket, and having a high level of turbulence intensity, was chosen for spectral analysis of velocity fluctuations. A simple single-wire hot wire probe, oriented normal to the streamwise direction, was used for all turbulence velocity measurements. The anemometer output was observed on an oscilloscope to contain very high frequencies. One might worry that the delay time might not be short enough for all the frequencies of interest to be covered below the folding frequency. But if the high frequency components of the signal do not contribute much energy to the velocity fluctuations, a longer delay time is tolerable. The minimum program delay time in this study was 0.6 msec, which gives a folding frequency of 830 cycles per second. In each run, 200,000 samples were taken, with maximum lag of 600 samples; hence there were 666 degrees of freedom. With a 95% confidence level, the estimate was within 0.465 db of the ture value. In order to test the adequacy of the 0.6 msec delay time, experiments were performed on the 24-inch model with five different discharges; each experiment was made twice, once with a 0.6 msec delay time, and again with a 1.0 msec delay time. The results were found to agree closely.

Five different discharges were used in the 24-inch model for spectral analysis. The plots of the spectral density functions are shown in figure 9. In all cases the area below the spectrum curve is unity to within 0.5%. The experimental points all fall on the same curve, as was the

case with the results of spectral analysis of pressure fluctuations performed in the water model (figure 5). No systematic difference can be found for different discharges. Among the five different discharges investigated, one was in the range of unstable flow patterns. In this case the high velocity core was deflected down into the scour hole by small disturbance elements placed at the entrance.

In the 9.6-inch model, six different discharges were studied. The results of spectral analysis are shown in figure 10. Also plotted in figure 10 is a curve representing the mean of the spectra from the larger model. Differences between all spectra shown in figure 8 are apparent in the low frequency range. The differences are such that spectra for lower Reynolds number flows exhibit relatively higher energy densities at low frequencies.

Loosely packed spherical particles forming the bed of the scour hole to not prevent local velocity fluctuations normal to the boundary, and they are also a source of eddies. It was suspected that the turbulence of the flow over the smooth concrete model used in this study might not adequately represent the turbulence structure near the boundary in an actual scour hole, because the rough beeds had been replaced by smooth impermeable concrete. To study the effects of beads on the experimental results, two layers of glass spheres were glued to the concrete bed profile. Velocity and turbulence intensity distributions were measured again for four different discharges. The results (figures 11a and 11b) show that the increase of roughness of the bed made the entrance velocity almost uniform. The high velocity core was deflected down into the scour hole only when the entrance velocity was less than 19.0 fps; when the entrance velocity was greater, separation from the lower boundary occurred, and a large eddy formed in the scour hole. As the discharge was further increased, the high velocity core tended to move downward again. Whether there was a discharge large enough to suppress the eddy completely was not ascertained because of the limited power of the blower.

Seven different discharges were used for spectral analysis in the model with the particle-covered bed. The spectra are shown in figure 12 and can be fitted onto two curves; one for cases in which the high velocity core went down into the scour hole, one for cases where the high velocity

core separated from the bed. There is a slight difference between these two spectra; relatively more energy was contributed by the medium size eddies when the high velocity core separated from the lower boundary.

By comparing spectra for the two types of bed for the case with no flow separation, figures 10 and 12, it is clear that the turbulence structure is virtually unaffected by the permeability or roughness of the scour hole profile.

F. Discussion. The stated aim of the flow-structure investigation was to ascertain whether the Reynolds number effect on the scour rate resulted from significant changes in the unsteady features of the flow. From the spectra presented in figures 6, 9, 10, and 12, the only significant anomalies are seen to be:

(i) between separated and non-separated flow, with eddies of medium frequency more pronounced in the separated flows,

(ii) between high and low Reynolds number flows, the eddies of low frequency being more pronounced at low Reynolds numbers.

Neither of these observations is capable of being reconciled with the earlier observations on the effect of Reynolds number on the scour rate. Flow separation was not observed in the scour experiments, so the relevance of the first point must be discounted. The second point suggests that low Reynolds number flows concentrate the energy of turbulence into a frequency range where particles should respond to turbulent agitation, and thus be more readily displaced from the bed. A trend in this direction is contrary to the trend observed in the scour experiments. Viscous effects, then, do not produce changes in the turbulence structure which explain diminished scour rates observed at low Reynolds numbers.

Possibly the most relevant observation concerns the extraordinary sensitivity of scour rate to temporal or spatial perturbations in the incoming jet. Figure 4 illustrates the point. The apparent anomalies between figures 2 and 3 might be ascribed to a similar phenomenon; experiments plotted in figure 3 were carried out after the system of screens and filters in the headtank had been modified for the hot-wire work. Superior stilling was

thereby achieved, but the rates of scour shown in figure 2 could no longer be reproduced. Thus, headtank geometry and approach flow conditions appear to be of prime importance in determining the scour rate and absolute scour depth.

We may extend the argument to the rate of the contraction between the headtank and the erodible bed; the geometry of the contraction changed markedly from one extreme model scale to the other, because no attempt was made to change its absolute dimensions (except the jet opening) from one scale to another. One is led to conclude, therefore, that dissimilarities in different scale jets may have been sufficient to account for the variable scour rates observed in the set of otherwise identical models.

VI. CONCLUDING STATEMENTS

Repetitive experiments carried out with a setup representative of a typical hydraulic model of a rock-protected structure, designed to explore viscous scale-effect phenomena, led to the following conclusions:

1. The observed variations in the rate of scour as a function of Reynolds number occurs in a direction which is contrary to that indicated by simple arguments based on the variation of particle drag coefficient with Reynolds number.

2. The effects of bed permeability or changes with scale of turbulence structure with Reynolds number do not allow the trend in scour rate to be rationalized.

3. The flow pattern is not governed in a wholly predictable way by boundary geometry; the Coanda effect may lead to variable patterns of jet trajectory.

4. Scour at a fixed value of the Reynolds number exhibits extreme sensitivity to temporal and spatial perturbations of the eroding jet.

5. Similarity in scour behavior can be expected only if strict geometric similarity is observed, not only in the vicinity of the eroding jet, but also in the region which determines the internal flow characteristics of the jet.

6. The results of these experiments suggest that Reynolds number scale effects are minimized if the Reynolds number, based on the particle size and mean flow velocity, is greater than about 2.5×10^3.

REFERENCES CITED

[1] Mehrotra, S.C., "Scale Effects in Model Tests of Rock-Protected Structures," Thesis submitted to The University of Iowa in partial fulfillment for the degree of Master of Science, Department of Mechanics and Hydraulics, June 1967.

[2] Chang, Y.C. "Spectral Analysis of Pressure and Velocity Fluctuations in a Submerged-Jet Scour Model," Thesis submitted to The University of Iowa in partial fulfillment for the degree of Master of Science, Department of Mechanics and Hydraulics, February 1969.

[3] Rouse, H., "Laboratory Instruction in the Mechanics of Fluids," *State University of Iowa*, Studies in Engineering Bulletin 41, 1961.

[4] Laursen, E.M., "Observations on the Nature of Scour," *Proc. Fifth Hydraulics Conference, State University of Iowa*, Studies in Engineering Bulletin 34, 1953.

[5] White, C.M. "Equilibrium of Grains on Bed of Stream," *Proc. Royal Soc. of London*, Vol. 174A, 1940.

[6] Glover, J.R., "Old Gold Model, Type 4-2H Hot-Wire Anemometer and Type 2 Mean-Product Computer," *Iowa Institute of Hydraulic Research*, Report No. 105, July 1967.

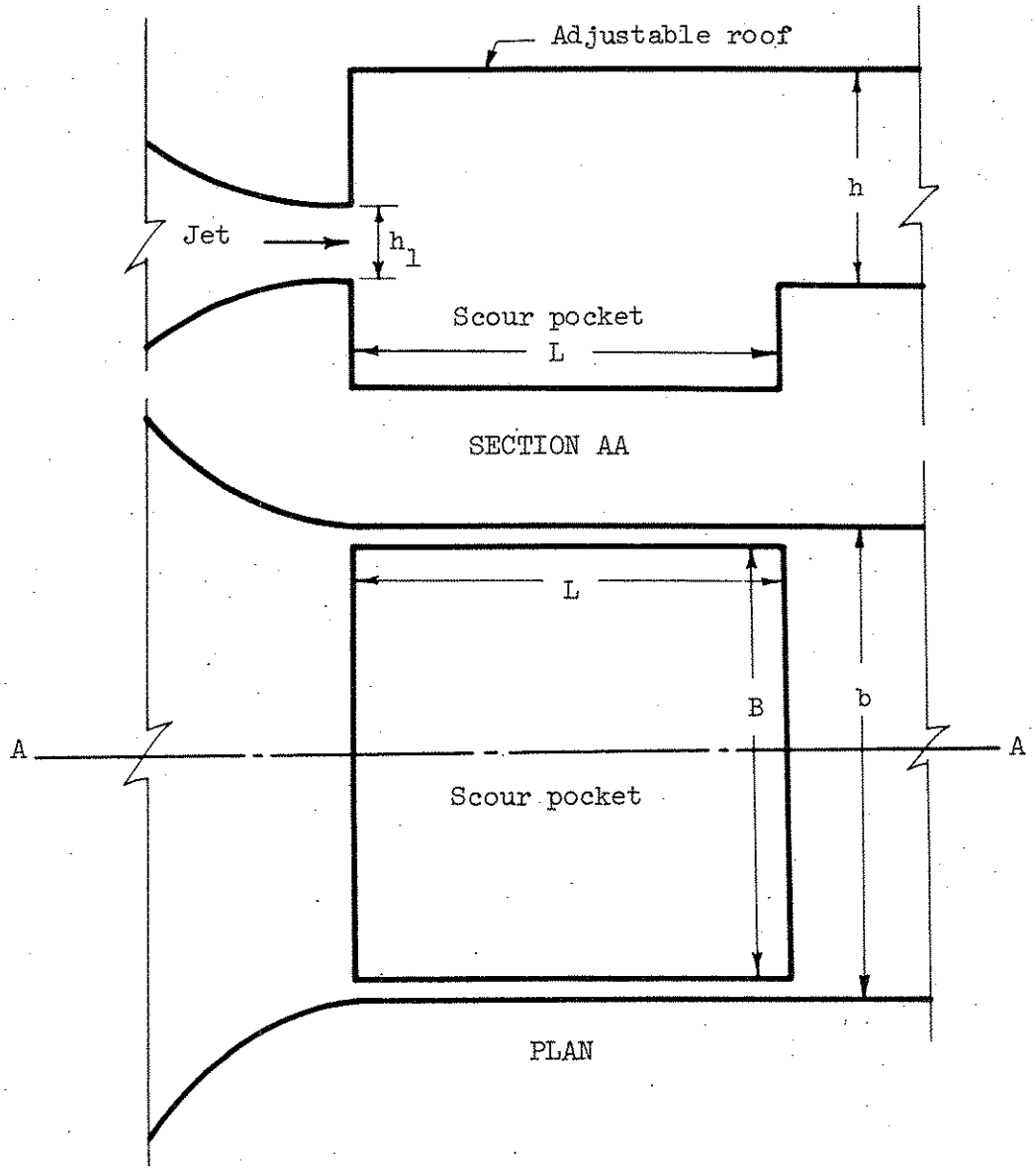

$L = 2h = 6h_1 = B = 40.6d$

Note: For 12.7 m.m & 15 mm beads $B \neq L$; $B = b$

Figure 1. Definition Sketch for Scour Model.

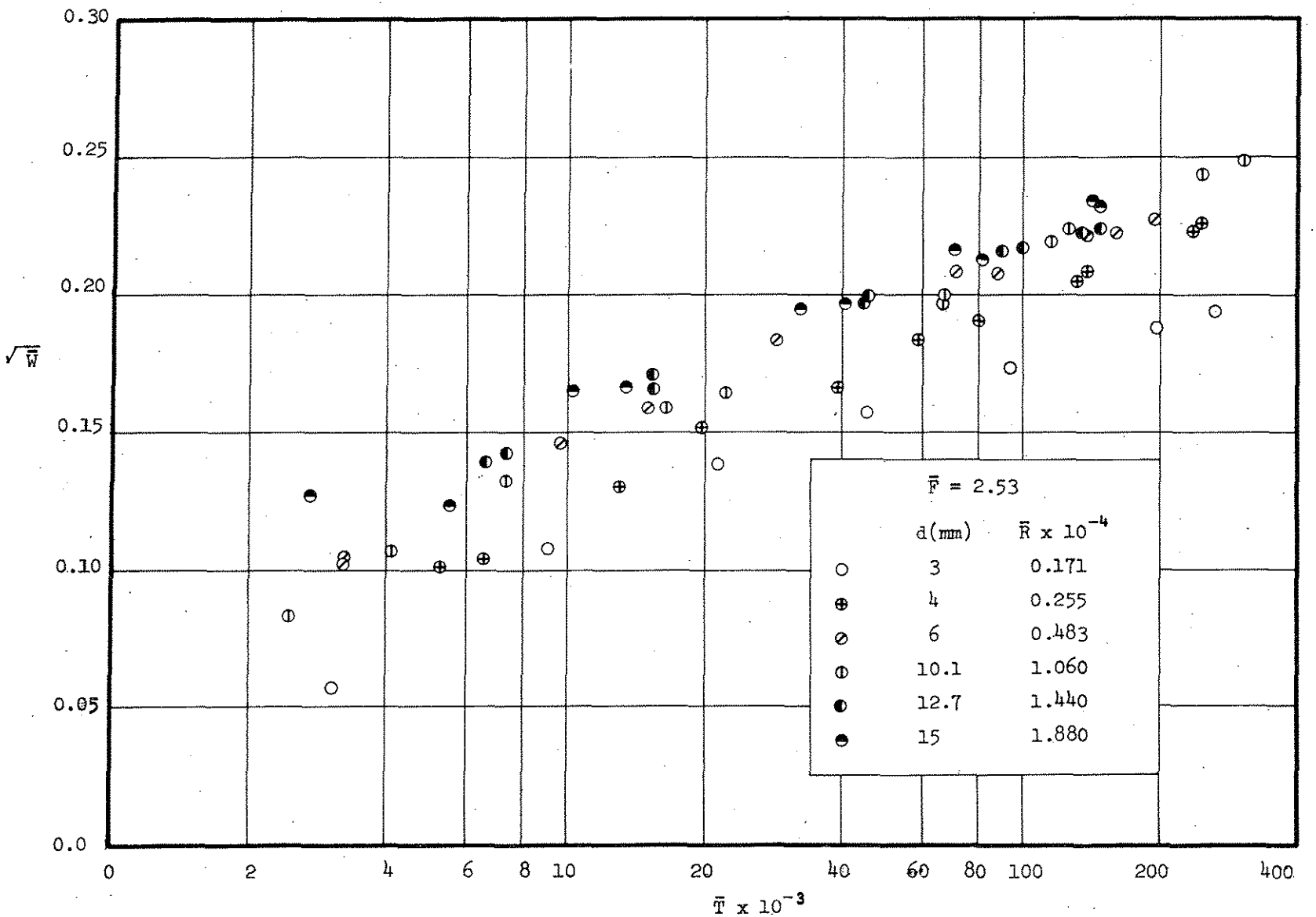

Figure 2(a). Variation of Normalized Depth of Scour with Normalized Time.

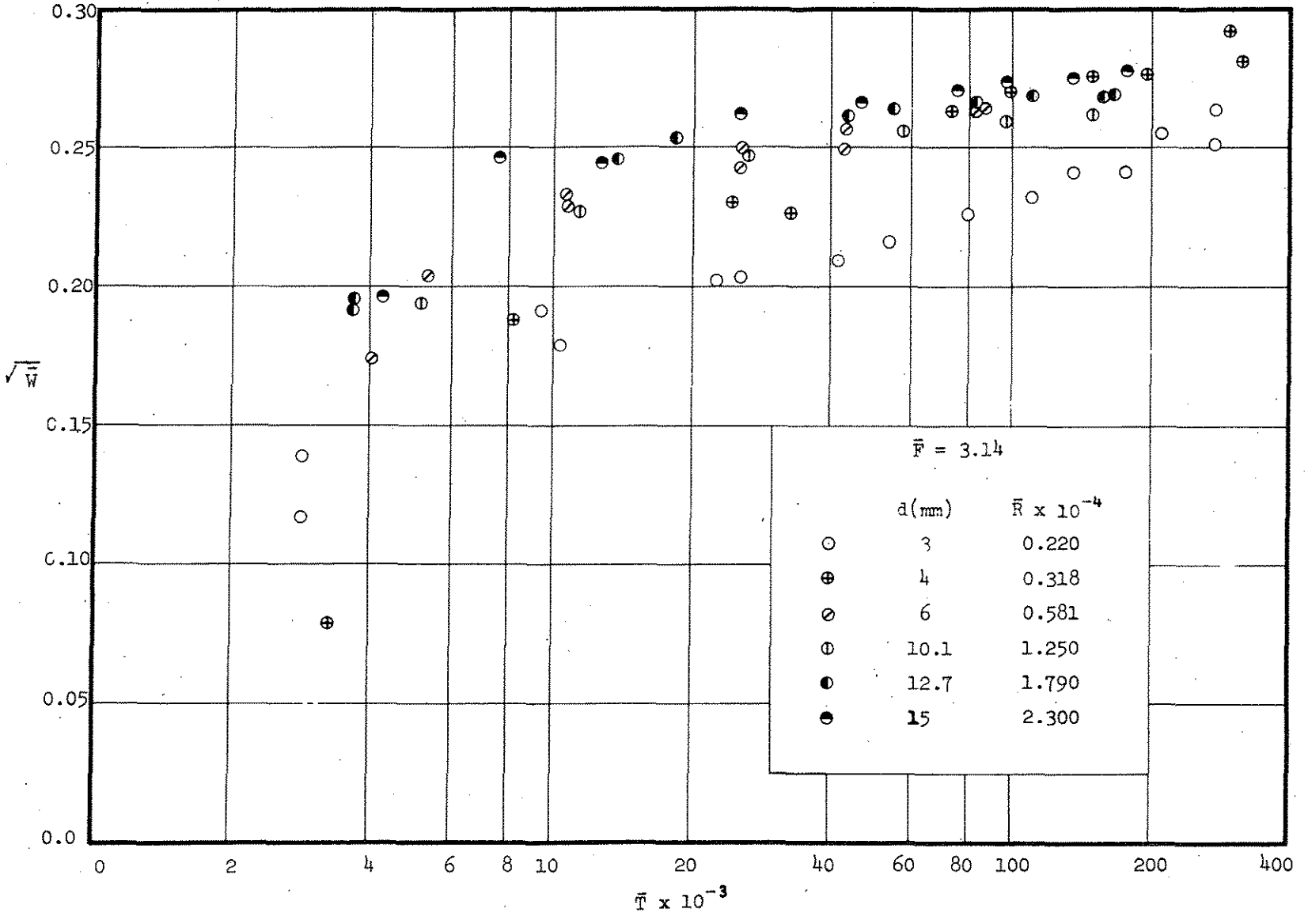

Figure 2(b). Variation of Normalized Depth of Scour with Normalized Time.

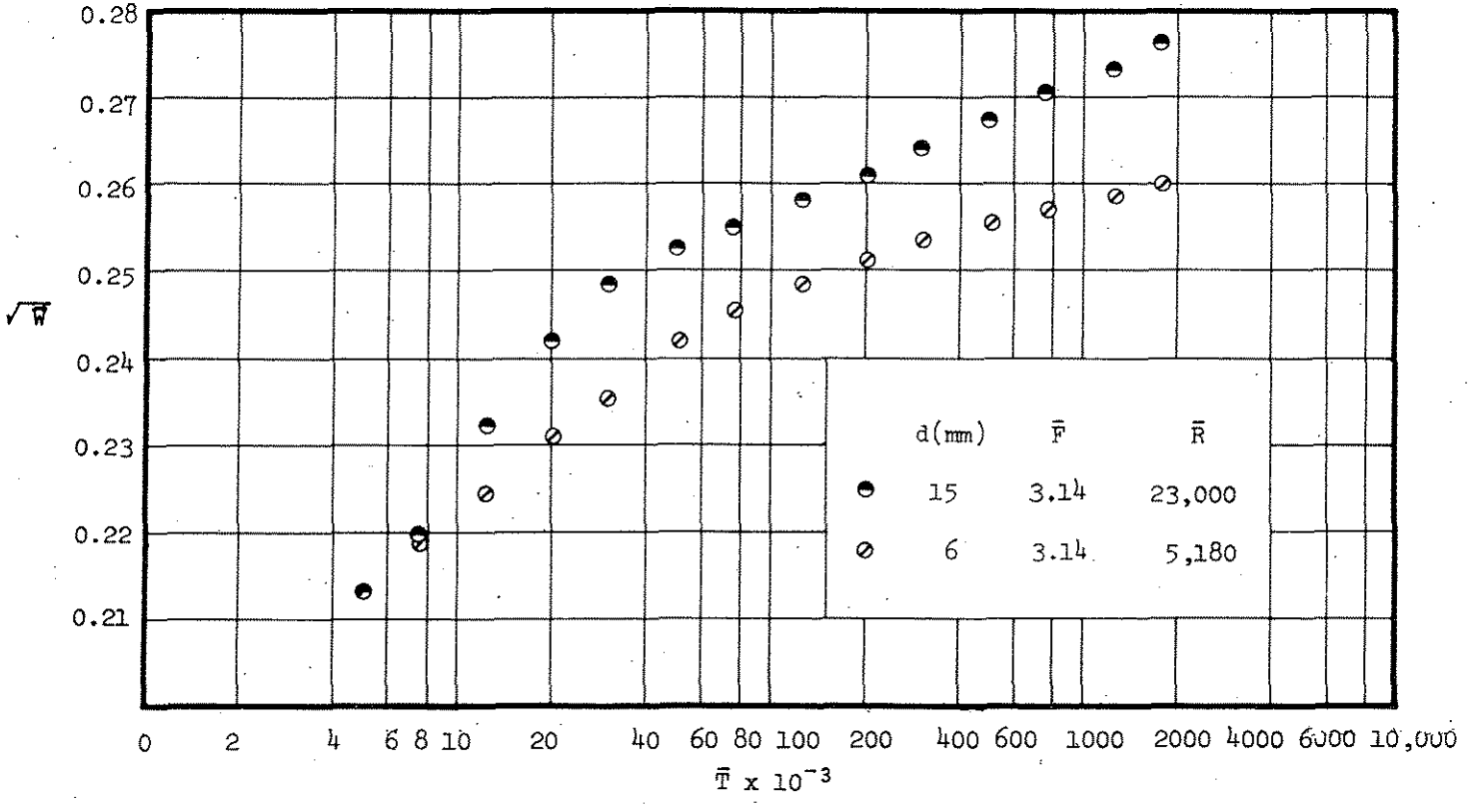

Figure 3. Long Term Normalized Depth of Scour.

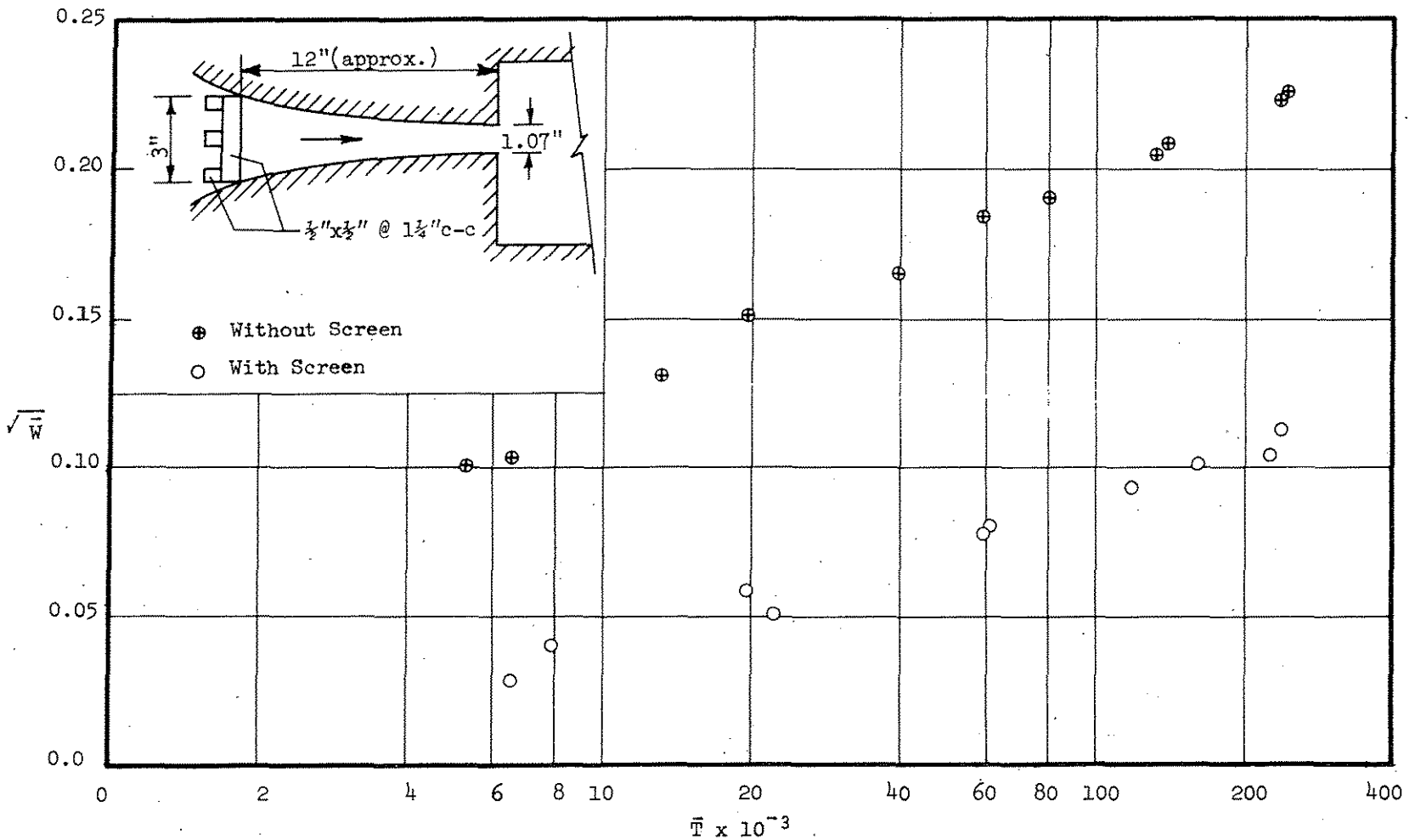

Figure 4. Effect of Screen on Normalized Depth of Scour.
d = 4 mm, $\bar{F}$ = 2.53, $\bar{R}$ = 2,550

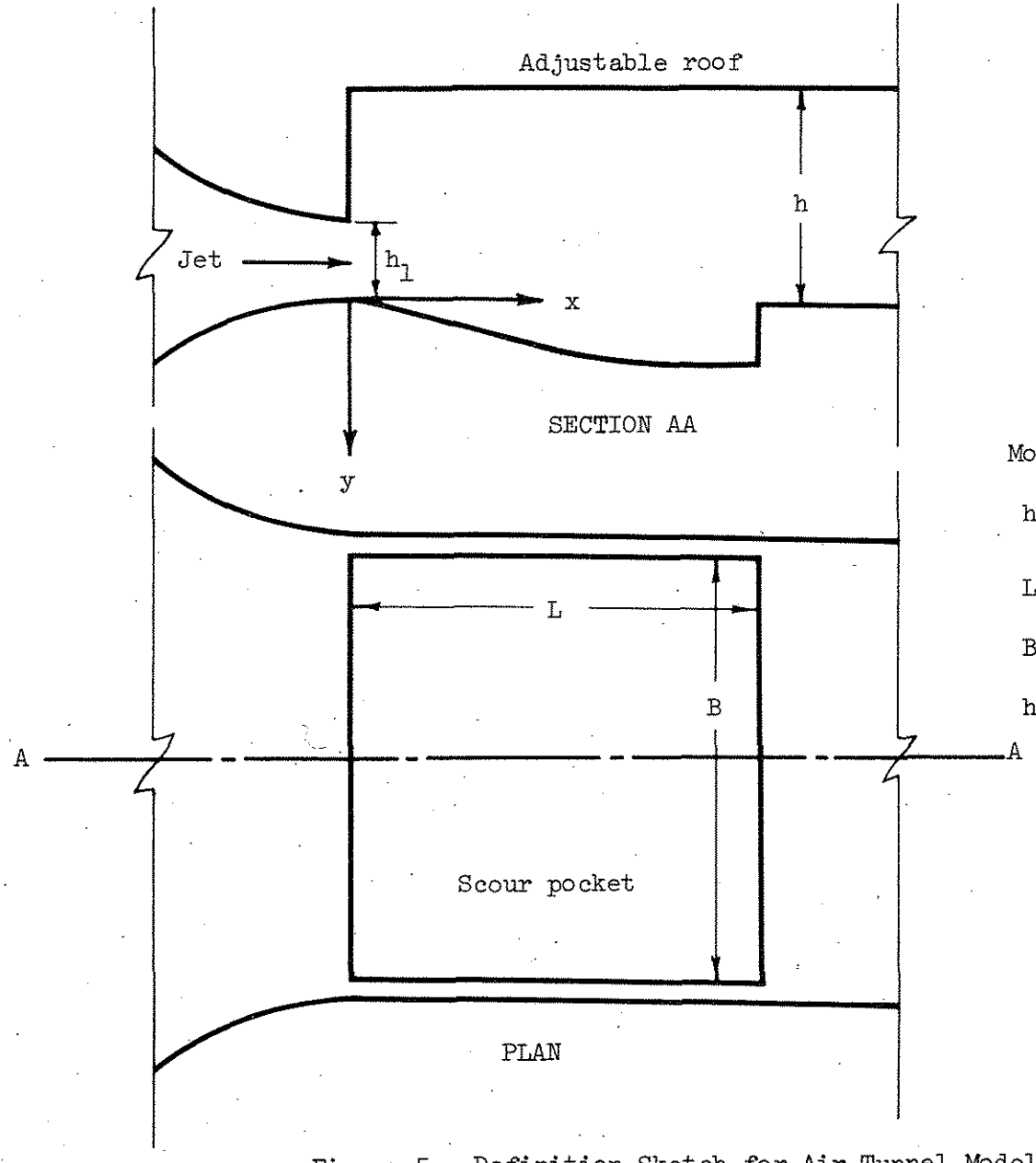

Model	24.0"	9.6"
h_1	4.0"	1.6"
L	24.0"	9.6"
B	18.5"	9.6"
h	9.0"	3.6"

Figure 5. Definition Sketch for Air-Tunnel Model.

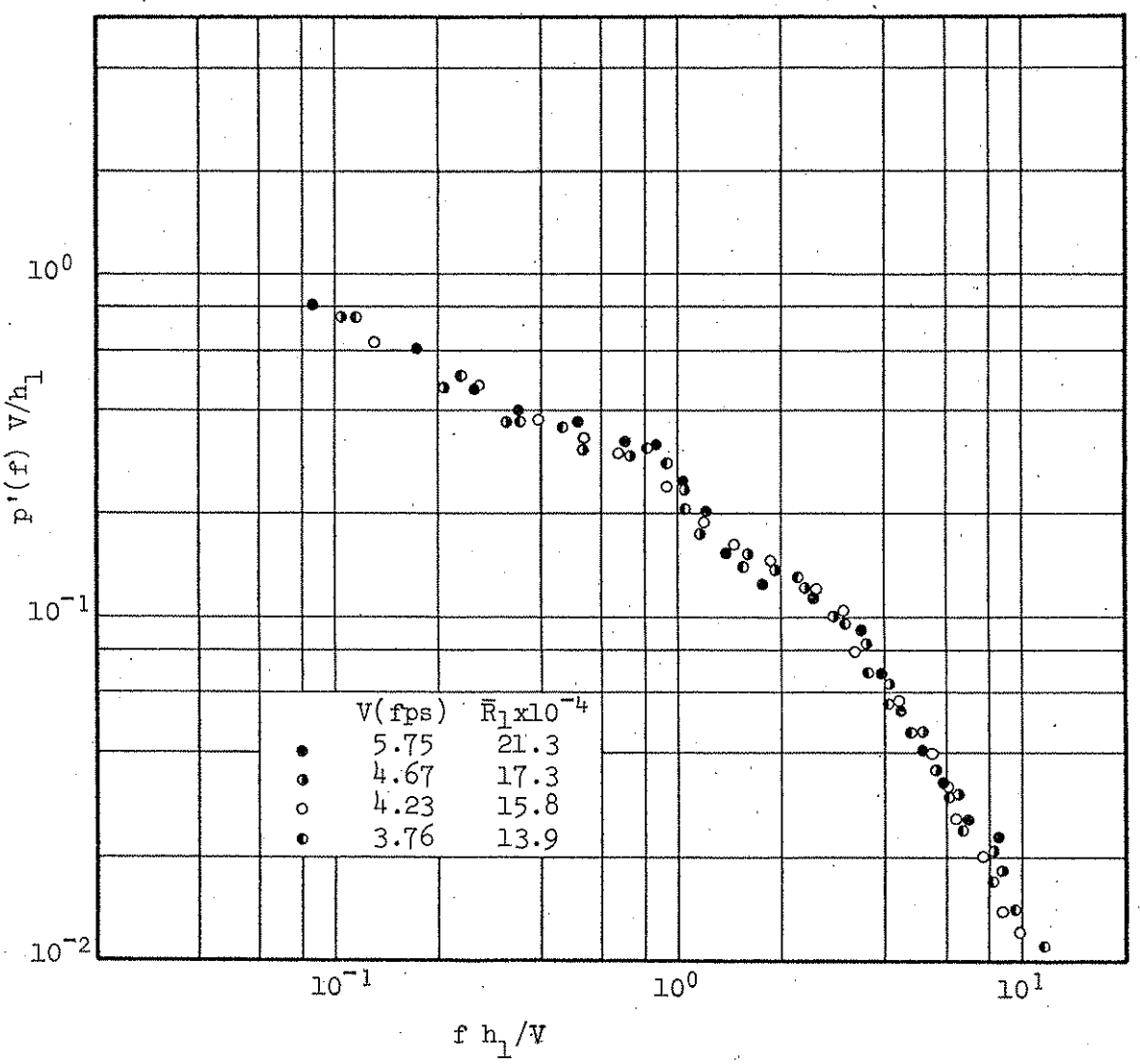

Figure 6. Spectra of Pressure Fluctuations for Five Different Discharges, Water Model.

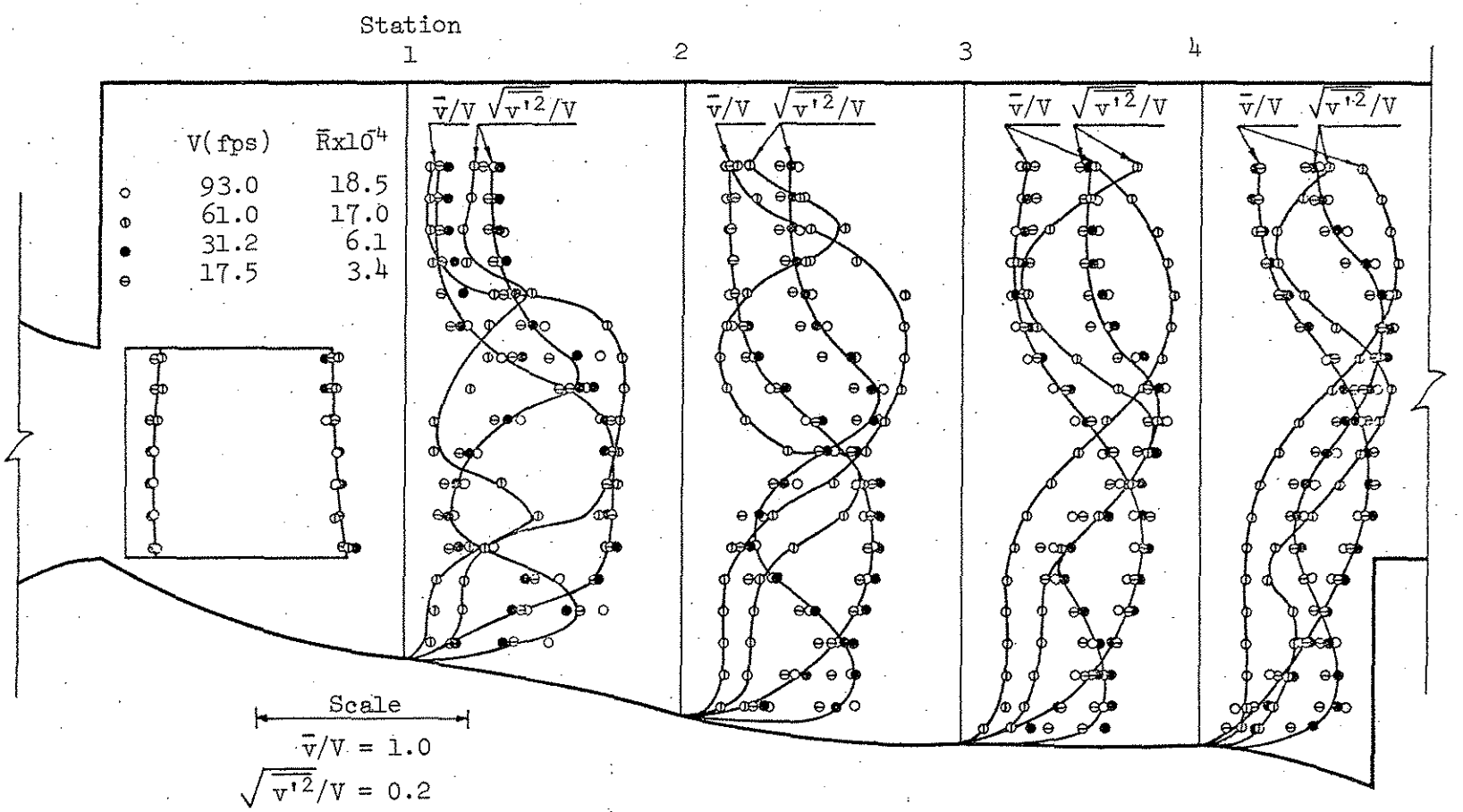

Figure 7. Velocity and Turbulence Intensity Profiles for 24-Inch Smooth-Bed Model.

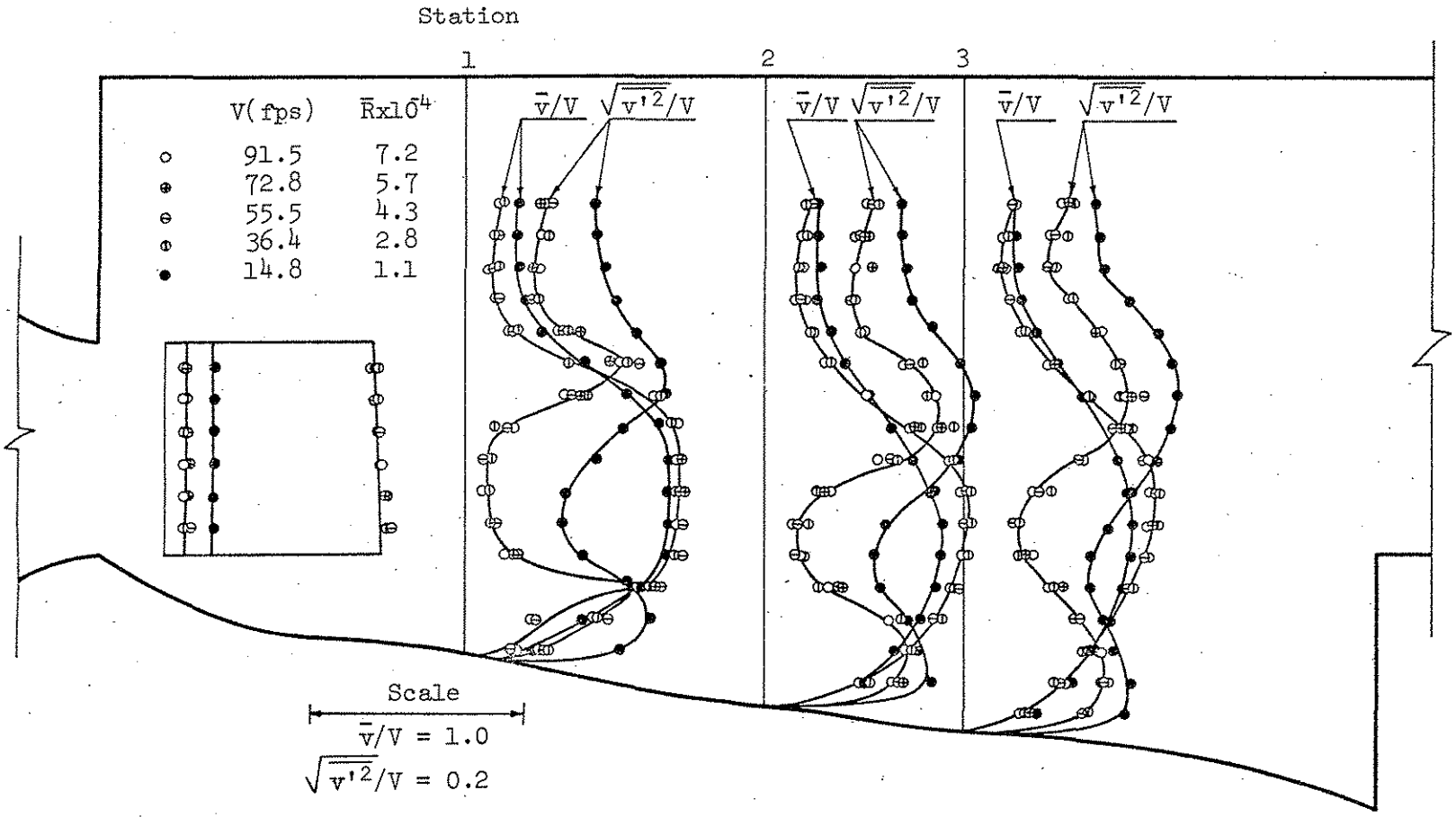

Figure 8. Velocity and Turbulence Intensity Profiles for 9.6-Inch Smooth-Bed Model.

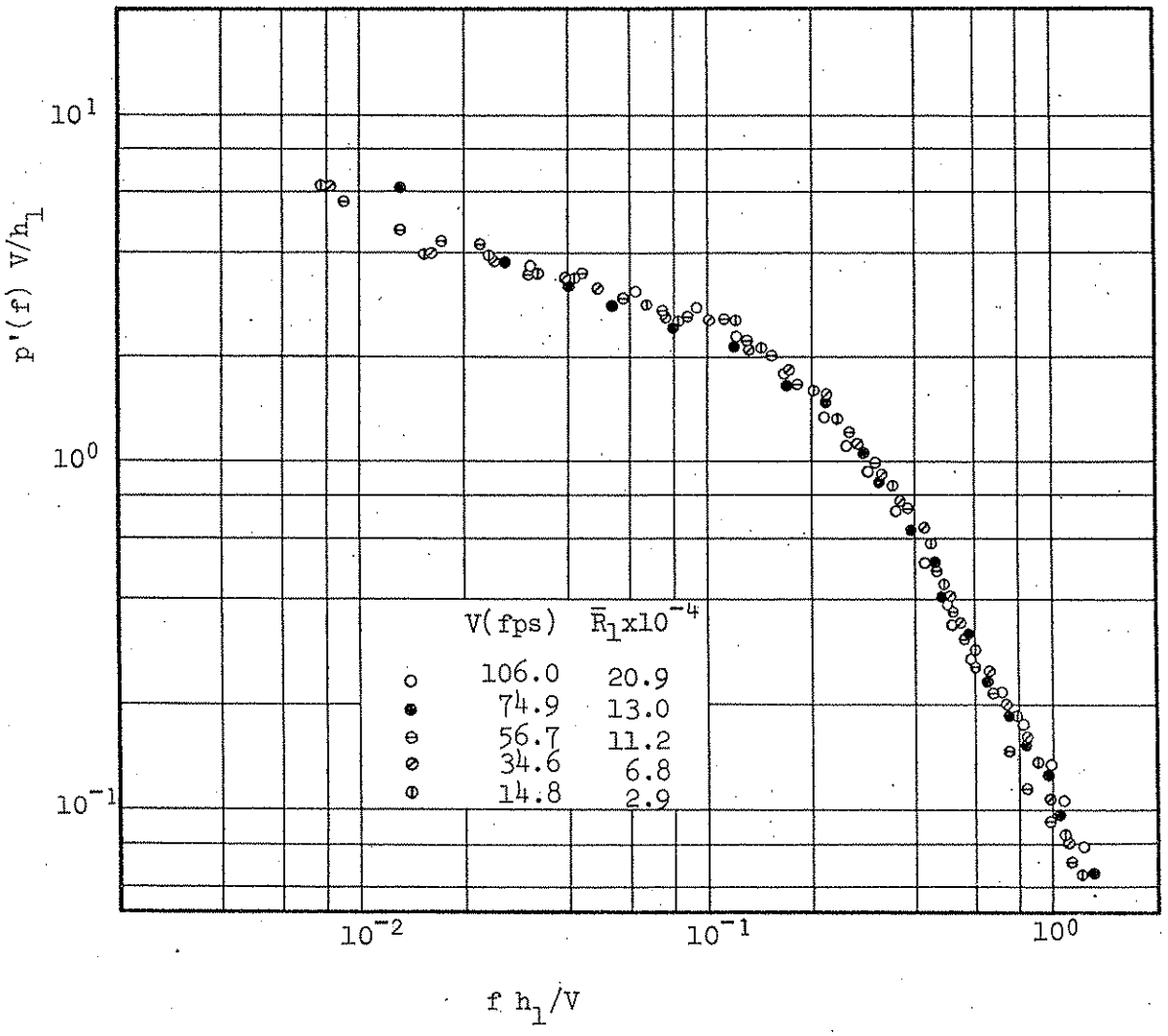

Figure 9. Spectra of Velocity Fluctuations for Five Different Discharges, 24-Inch Smooth-Bed Model.

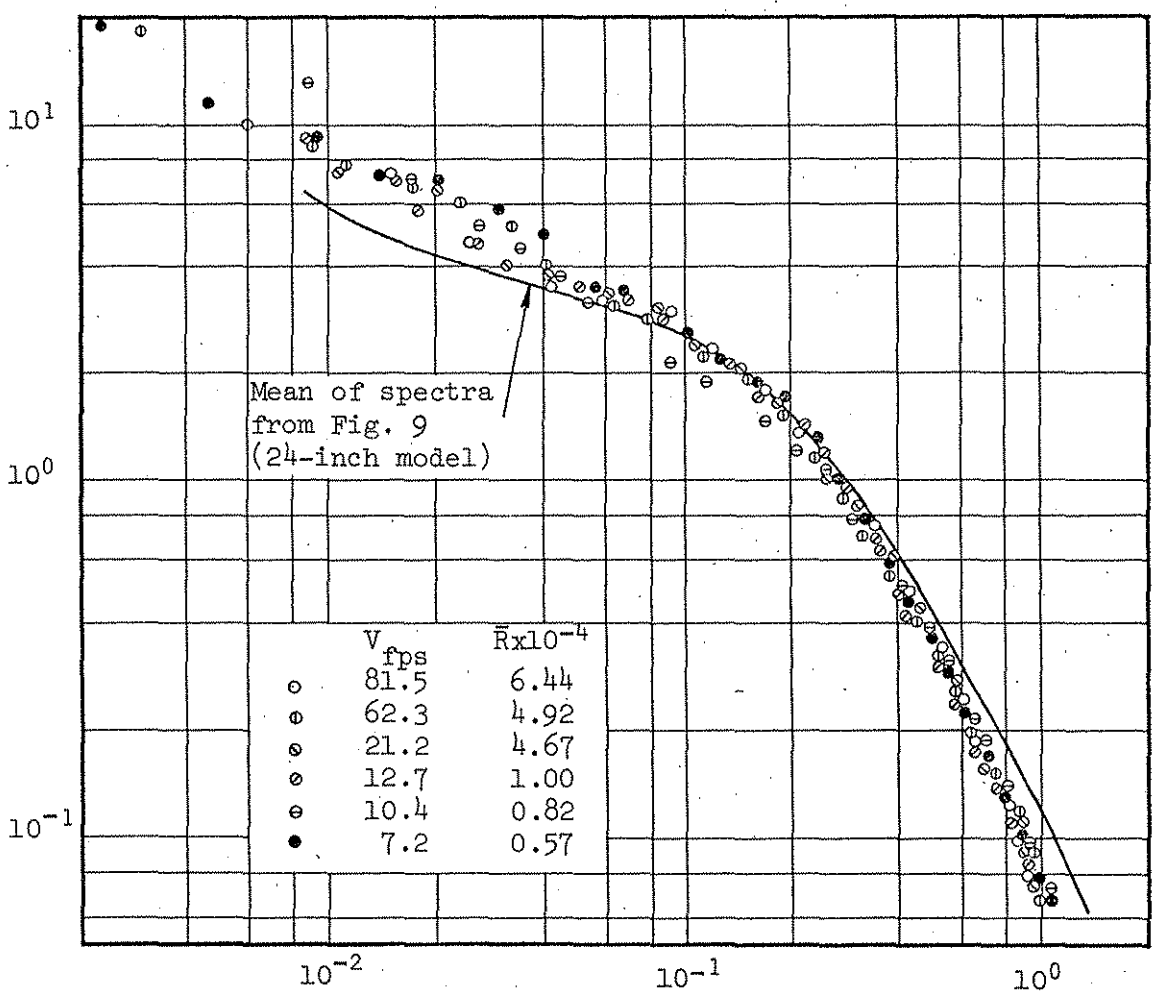

Figure 10. Spectra of Velocity Fluctuations for Six Different Discharges, 9.6-Inch Smooth-Bed Model.

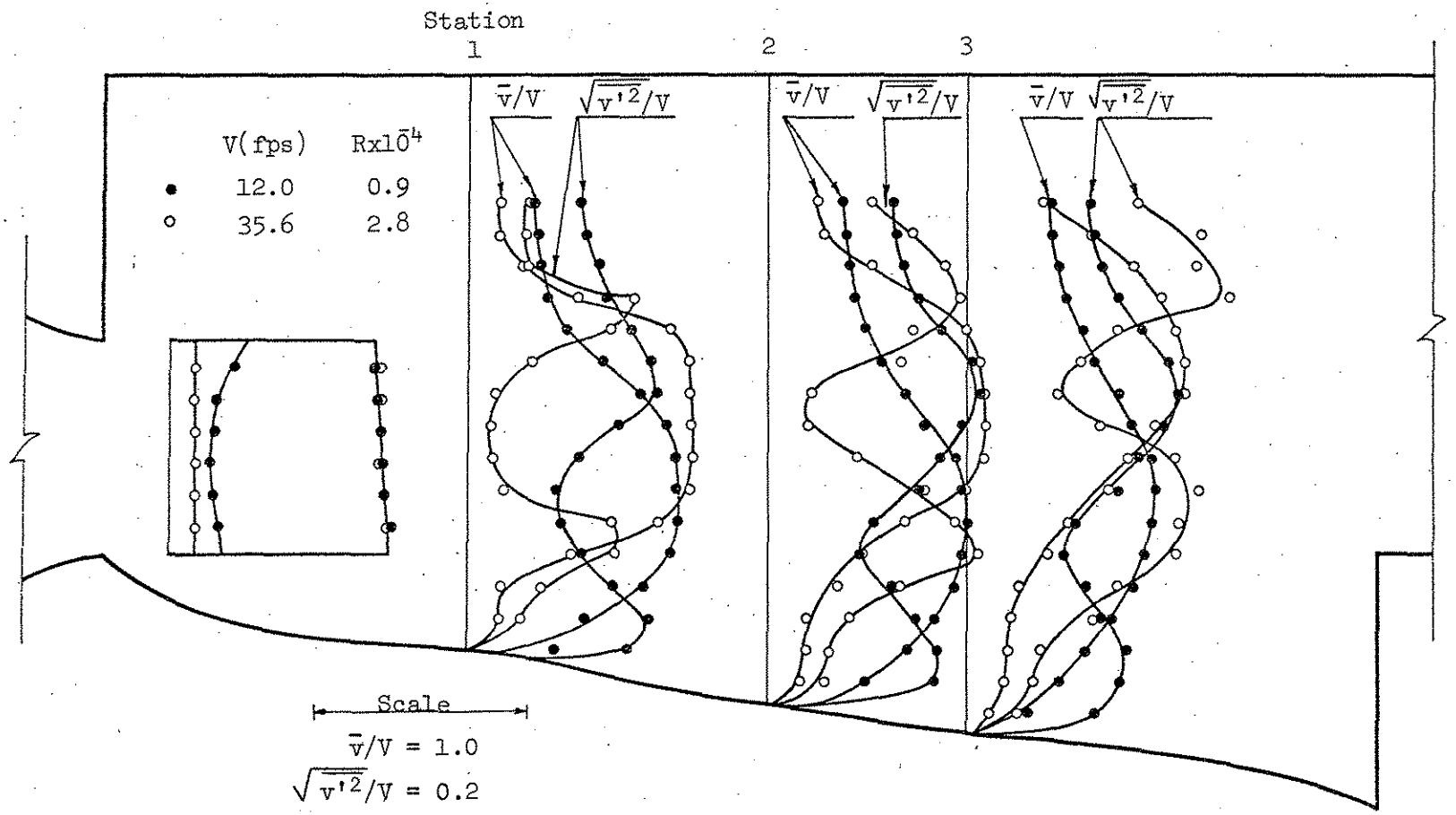

Figure 11(a). Velocity and Turbulence Intensity Profiles for Two Different Discharges, 9.6-Inch Marble-Bed Model.

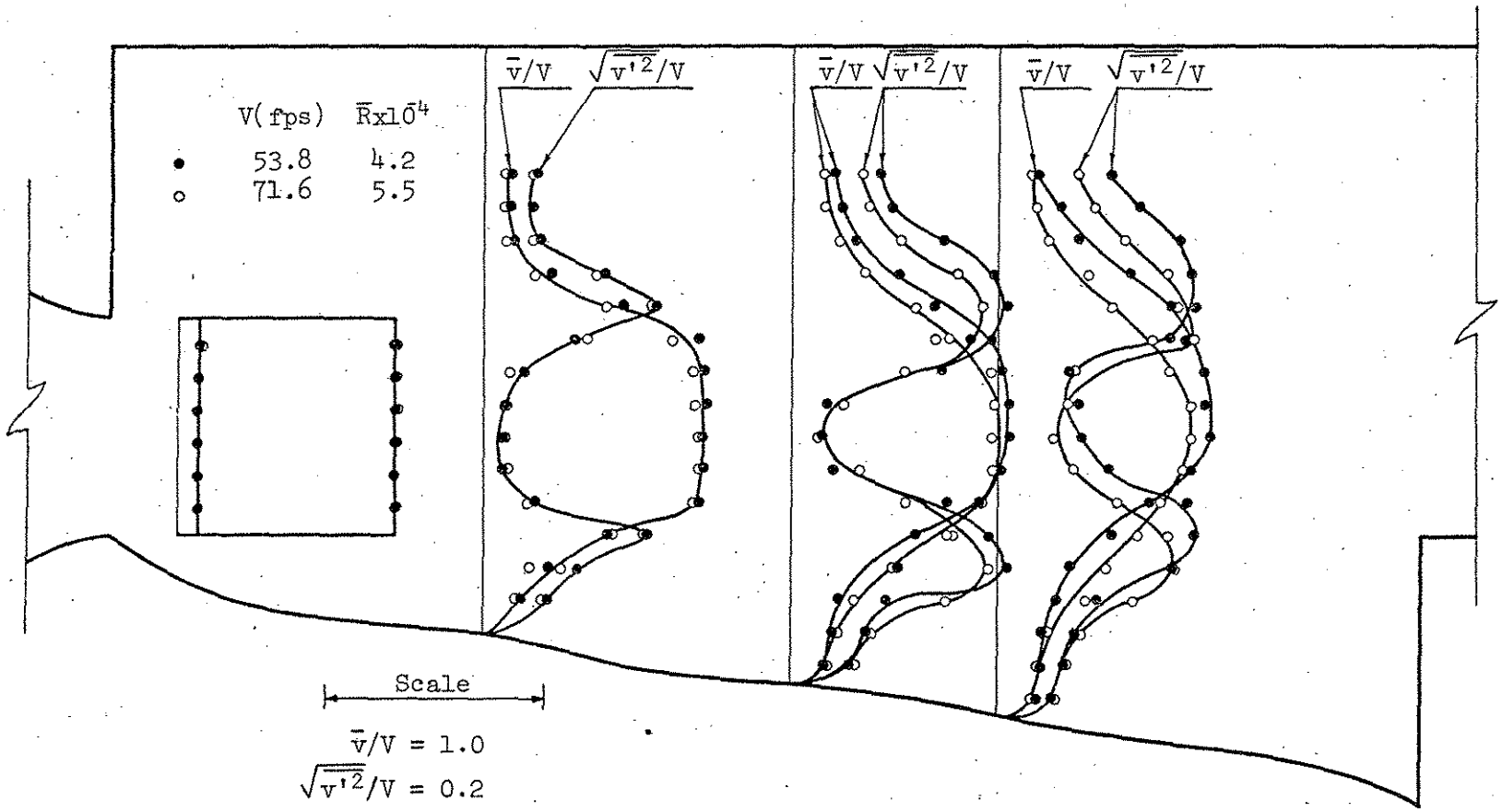

Figure 11(b). Velocity and Turbulent Intensity Profiles for Two Different Discharges, 9.6-Inch Marble-Bed Model.

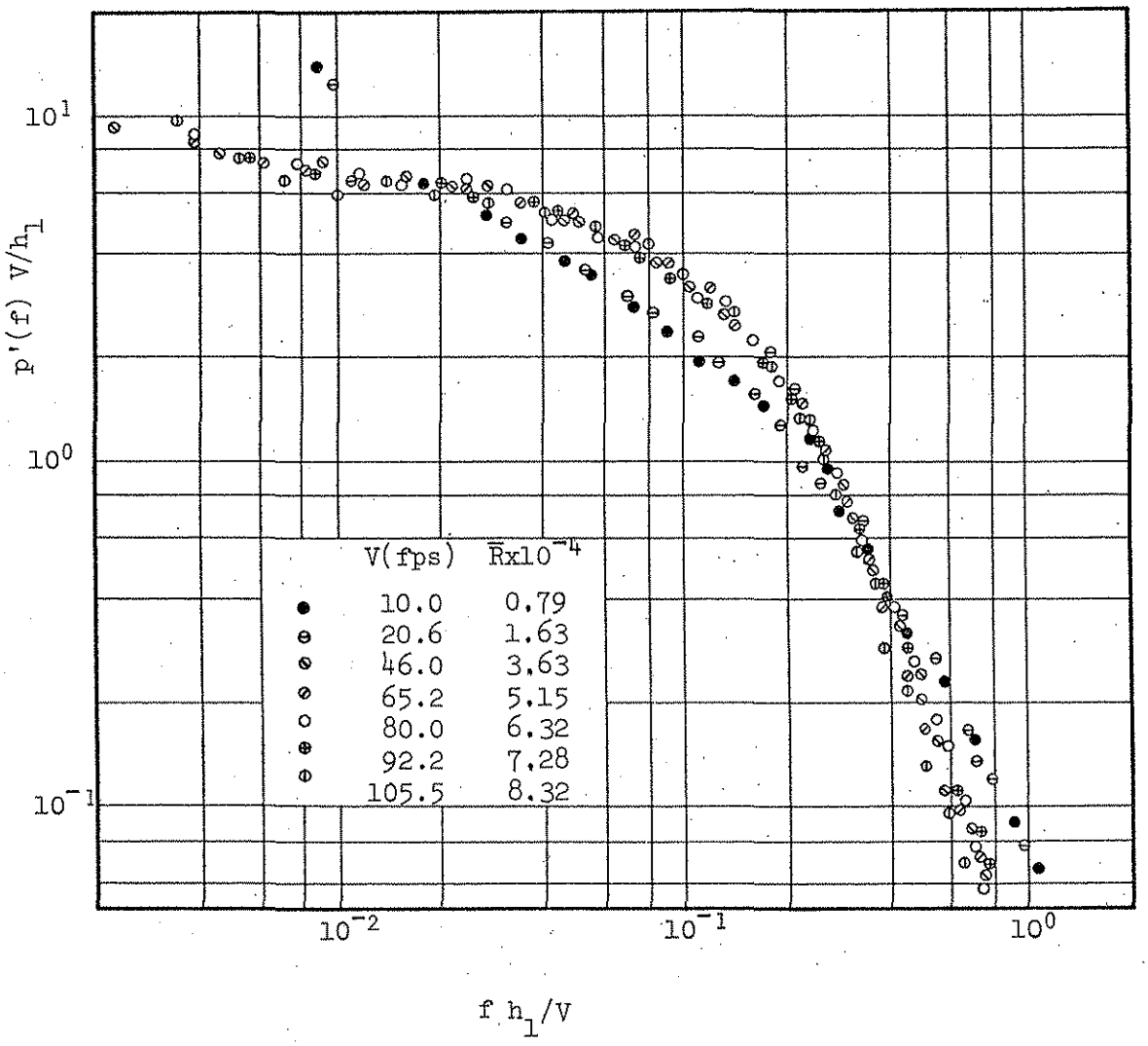

Figure 12. Spectra of Velocity Fluctuations for Seven Different Discharges, 9.6-Inch Marble-Bed Model.